Microfluidics and Nanofluidics (2021) 25:51
https://doi.org/10.1007/s10404-021-02450-x

RESEARCH PAPER

Focused ion beam milling based formation of nanochannels in silicon-glass microfluidic chips for the study of ion transport

Denis Lebedev[1,2,3] · Grigory Malyshev[4] · Ilya Ryzhkov[5] · Alexey Mozharov[1] · Konstantin Shugurov[1] · Vladislav Sharov[1,6] · Maxim Panov[2] · Ilya Tumkin[2] · Polina Afonicheva[3] · Anatoly Evstrapov[3] · Anton Bukatin[1,3] · Ivan Mukhin[1,4]

Received: 24 March 2021 / Accepted: 8 May 2021 / Published online: 31 May 2021

Abstract

Nowadays nanofluidic devices have a great potential in biosensing and DNA sequencing applications. This work is aimed at development of the technique for fabrication of arrays of nanochannels in silicon-glass chips by focused ion beam milling. The use of lithography with charged particles (electrons and ions) paves the way for the fabrication of micro- and nanochannels and pores as well as functional nanostructures of a more complex shape in nanofluidic devices. In this study, a technique for fabrication of microfluidic chips with a system of nanochannels connecting two independent volumes (2 half cells) was developed. It was shown experimentally that the focused ion beam etching time has an influence on both the width of the created nanochannels and their depth. We suggested using anodic bonding of a silicon wafer with the net of micro- and nanochannels with a glass plate for encapsulation of such devices that provide their long lifetime of microfluidic devices. To determine the functionality of the produced devices we studied the ionic conductivity of the produced nanochannels experimentally and using a theoretical approach. Analyzing the results, we determined the effective diameter of the nanochannels and the surface charge density inside the channel which were 20 nm and 1.5 mC/m^2, respectively. The proposed technique allows to create ensembles of channels with a predefined width and depth. Such systems can find wide application in studies of the transport phenomena of both ions and various molecules in nanofluidic devices.

Keywords Nanochannels · Nanopores · Focused ion beam · Lithography · Ion transport · Microfluidic device · Nanofluidic device

1 Introduction

Recently, researchers have had the opportunity to study various processes at the micro- and nanoscale due to the technological development of micro- and nanodevice fabrication techniques (Ramsden 2016). The rapid development of these technologies gives the opportunity to integrate nano-sized elements such as nanopores, nanochannels or nanoslits into microfluidic devices and turn them into nanofluidic devices (Evstrapov et al. 2012; Mukhin et al. 2015). This incorporation allows to study biophysical and biochemical processes at a qualitatively new level and have various applications, including DNA analysis and sequencing (Wang et al. yyy; Kurita and Niwa 2016), amplification and concentration techniques (Zhang et al. 2019; Ouyang and Han 2019), protein studies (Medina-Sánchez et al. 2016), electrophoresis (Ou et al. 2020), development of chemical and biochemical sensors (Le et al. 2020; Hou et al. 2013; de la

✉ Denis Lebedev
denis.v.lebedev@gmail.com; d.v.lebedev@spbu.ru

1 St. Petersburg Academic University, 8/3 Khlopina Street, St. Petersburg 194021, Russia

2 Saint Petersburg State University, 7/9 Universitetskaya nab, St. Petersburg 199034, Russia

3 Institute for Analytical Instrumentation RAS, 26 Rizhskii pr, St. Petersburg 190103, Russia

4 ITMO University, 9 Kronverksky pr, St. Petersburg 197101, Russia

5 Institute of Computational Modelling SB RAS, 50/ 44, Akademgorodok, Krasnoyarsk 660036, Russia

6 Ioffe Institute, 26 Politekhnicheskaya, St Petersburg 194021, Russia

Escosura-Muñiz and Merkoçi 2012) and etc. One of the key points of using nanopores and nanochannels as an analytical tool is the understanding of molecular and ionic transport in the nanostructures. These studies are important from the fundamental point of view, as well as for specific practical applications in the field of biomedicine (Ouyang and Han 2019; Shi et al. 2018) and genetic engineering (Noakes et al. 2019). Moreover, such microfluidic systems containing nanopores and nanochannels are of great interest (Zhu et al. 2019) for selective transport and separation of ions and molecules (Wang et al. 2018; Xu et al. 2018) and electrochemical energy conversion (Hao et al. 2020). It is very promising to create nanofluidic devices, which principle is based on the effect of ionic concentration polarization. Such systems find many applications both in the field of biomedicine and and component separation (Han and Chen 2019, 2020a, b, c).

Bioengineering technologies are one of the most promising applications of microfluidic devices, particularly in terms of fabrication of artificial (biomimetic) analogs of living nanofluidic systems (Kowalczyk et al. 2011). In living systems all electrical signals are carried by ions (anions and cations), compared to microelectronics, where electrons and holes are charge carriers. Biological nanochannels, such as ion channels, water channels and glucose transporters, can efficiently regulate the transport of ions/molecules across the cell membrane due to their geometric shape and protein composition of the surface (Payandeh et al. 2012; Favre et al. 1996). Thus, the fabrication of the artificial analogs of biological micro- and nanochannels and molecular pumps in cell membranes allows to effectively study the transport mechanisms in such systems, which is confirmed by the recent papers (Tagliazucchi and Szleifer 2015; Guan and Reed 2012). Moreover, the influence of the electromagnetic field and electric charges on the selectivity of such membranes and nanochannels separating electrolyte solutions with different concentrations is actively studied (Sparreboom et al. 2009; Picallo et al. 2013; Siria et al. 2013).

Various approaches can be implemented for the fabrication of artificial nanochannels in microfluidic devices (Xia et al. 2012; Chen and Zhang 2018). Among them, there are optical methods such as conventional photolithography (Mokkapati et al. 2011) and interference lithography (O'Brien et al. 2003) are very widespread. However, due to the optical nature of the fabrication processes, it is quite difficult to obtain nanochannels with sizes less than 50 nm, which is mainly limited by the wavelength of the UV source used. Other methods for nanochannel fabrication are based on nanotechnological processes, e.x. nanoimprinting (Guo 2007; Wu et al. 2012) or thin film deposition (Nam et al. 2010; Zhou 2011). Despite the complexity of the experimental procedures and high requirements for materials and qualification of the researches, these methods give the possibility to create nanochannels from different materials with a given geometry. There are also bottom-up methods that allow to use the physical properties of bulk materials to grow nanochannels. Usually these methods suggest creating nanochannels in polymer (Mills et al. 2010). Another class of nanochannels is track etched nanochannels in polymer films, they have been used intensively to study ion, molecule and nanoparticle transport (Ma et al. 2020), and have been used in various applications including biosensors (Ma et al. 2019a) and energy conversion (Ma et al. 2019b).

One of the most promising techniques for obtaining single nanochannels is the use of high-energy beams of charged particles (electrons or ions) (Chen 2015; Xu and Matsumoto 2015). Using this approach (especially focused ion beam (FIB) milling) it is possible to obtain channels of various geometries with a resolution of up to several nanometers (Menard and Ramsey 2011). However, for all of the discussed methods there is a problem of encapsulating the nanochannels after their fabrication. Conventionally, the encapsulation is performed by coating a pre-treated surface with a polymer (e.g., polydimethylsiloxane, PDMS) or by welding a solid substrate to a cover plate at high temperatures (McDonald and Whitesides 2002; Peng and Li 2016). However, these methods have disadvantages such as the short lifetime of the nanofluidic device in case of polymers or deformation of the channels during welding. The most detailed analysis of modern methods for fabricating nanochannels can be found in (Chen and Zhang 2018).

In this work, we demonstrate a comprehensive study of microfluidic chips with nanochannels, fabricated with the use of both photolithography and FIB milling, as well as the anodic bonding. Additionally, we investigated the ionic conductivity of the fabricated devices, which was supported by a one-dimensional theoretical model. Our results show that a combination of FIB milling and anodic bonding techniques allows to fabricate microfluidic chips with a service life extending several months. Such microfluidic devices provide reproducible ionic conductivity measurements that fit to the developed theoretical model.

The use of FIB milling opens up the wide opportunities for the creation of micro- and nanochannels and pores as well as functional nanostructures with a more complex shape. This approach paves the way to produce channels, where the electrical conductivity properties can be controlled. This is important for lab-on-a-chip systems with extended functionality and fields of application.

2 Result

2.1 Device fabrication

The fabrication of a microfluidic chip with a system of nanochannels requires a multi-stage complex approach.

At the first stage, it is necessary to determine the geometric parameters and shape of the device. To eliminate the effects of the concentration polarization of the working solution, its flows near the inlet and the outlet of the nanochannels should be provided. To meet this requirement, the X-shaped geometry of the channels was proposed. Two microchannels representing the two halves of the conventional letter X (the left and the right parts) were separated by a bridge of 10–15 μm width, where an array of nanochannels was subsequently formed. Each microchannel had an inlet and an outlet providing a two-way working solution flow in the system.

The fabrication steps of the developed microfluidic device are shown in Fig. 1. At the first step, the surface of a silicon wafer was oxidized to a depth of about 250 nm to have chemically and biologically inert material with the well-studied surface properties in different aqueous solutions. The oxidation process was performed at a temperature of 1100 °C alternately in a flow of dry oxygen and a mixture of oxygen and water vapor. After that optical lithography and plasma etching were used to fabricate X-shaped microchannels. The depth of these channels was 10 μm. In the bridge between the microchannels the set of about 20 nanochannels was made by FIB milling using a CrossBeam Neon40 (Carl Zeiss) crossed electron and ion beam system.

The obtained micro- and nanochannels were visualized and characterized by means of scanning electron microscopy (SEM) (Fig. 2). The SEM images show that the edge of the bridge between two microchannels didn't have a sharp step, but rather had a relatively gentle slope (showed Fig. 2b). Figure 2c, d show typical SEM images of the nanochannels that were formed in the bridge to connect the microchannels. Note, that due to the features of the plasma etching regime the angle of the sidewalls of the microchannels was not 90 degree. Therefore, the SEM images can provide the information only about the width of the nanochannels. Due to non verticality of the sidewalls of the bridge it's hard to determine their depth due to the relatively low resolution in the direction of the out of plane of scanning. Thus, we used atomic force microscopy (AFM) with a sharp silicon probe (HA-FM, NT-MDT SI Ltd.) for correct estimation of the depth of the nanochannels.

The FIB etching of the nanochannels was carried out across a single line with 1 pixel width and 15 μm length, exceeding the width of the bridge. To investigate how the FIB etching time influences the channels dimensions, this time varied from 2 to 60 s. If the etching time was less than 2 s, the channels' depth was nonuniform and not reproducible.

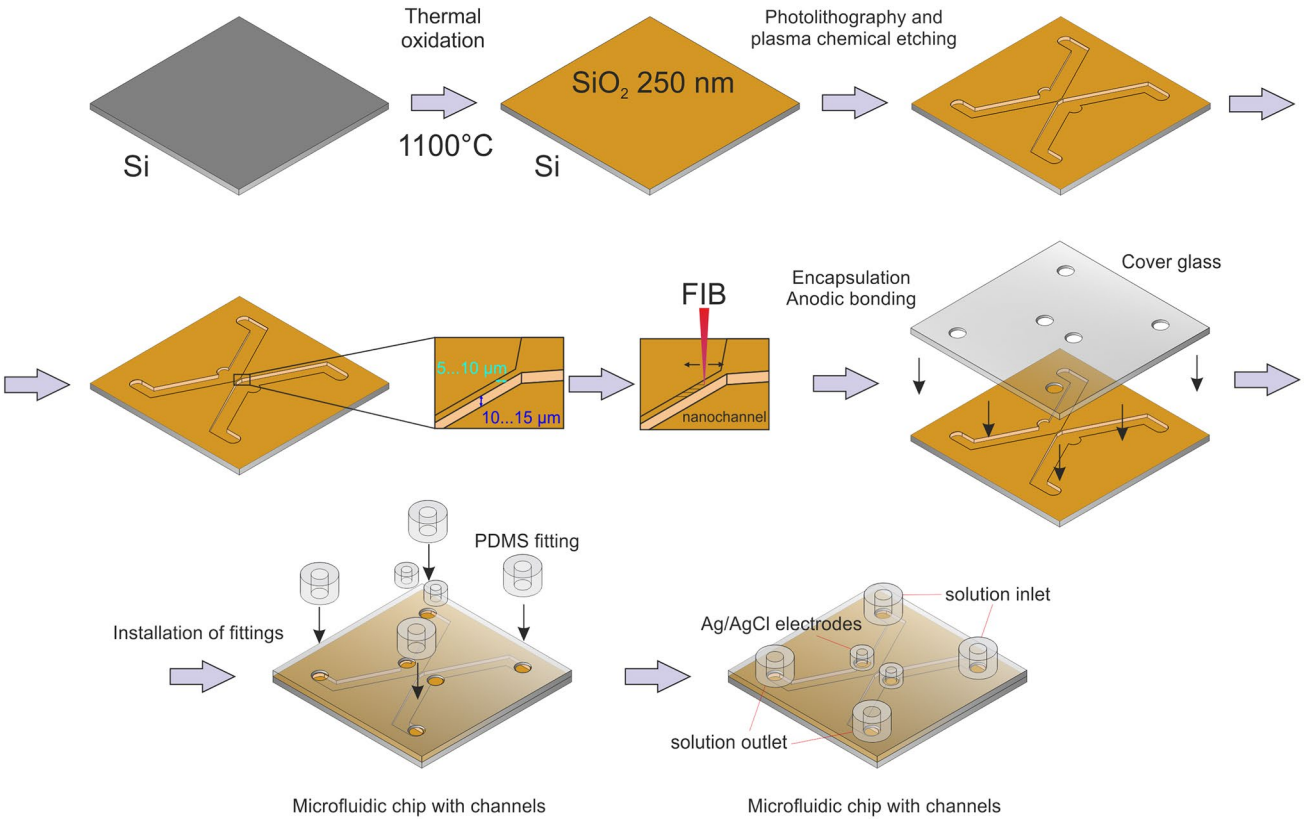

Fig. 1 The fabrication steps of a microfluidic device with nanochannels

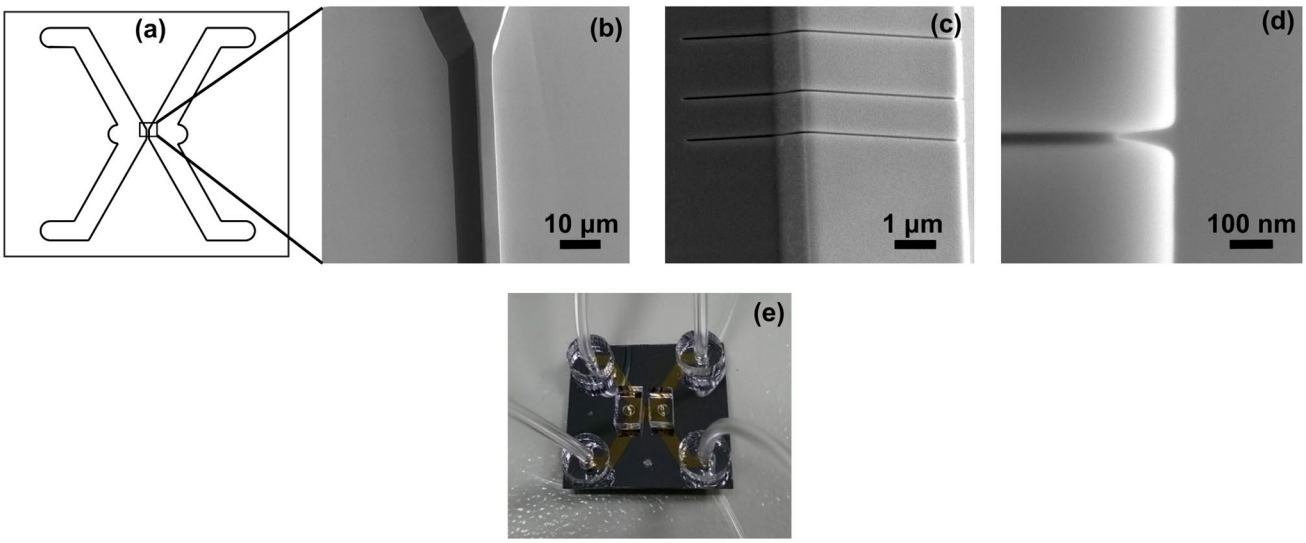

Fig. 2 **a** Microfluidic chip circuit, **b–d** images of the microfluidic channels obtained with a scanning electron microscope (SEM, isometric views), **e** photo of a general view of a microfluidic chip

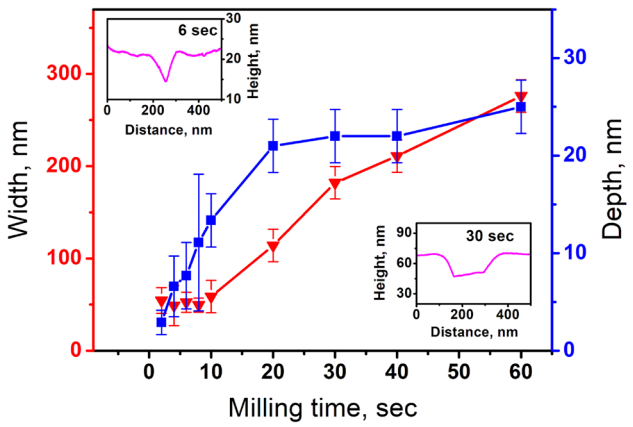

Fig. 3 AFM study of the nanochannel geometry from the FIB etching time. The width of the channels was measured at half of the depth. The bars show the standard error. The lines are guided by eyes. The insets show AFM profiles of a single nanochannel obtained at 6 s and 30 s milling time

In each device, we made at least 10 channels and the error in their dimensions was no more than 20% Fig. 3 shows the dependence of the nanochannels width on the FIB milling time. The cross-sections of the channels, demonstrated on the inserts on Fig. 3, obtained with the FIB milling time of 6 s and 30 s indicated that the nanochannels are wedge-shaped. For the etching times less than 10 s the width of the channels did not change significantly, when the channel width increased with close to the linear dependence. Additionally, Fig. 3 represents the dependence of the nanochannel depth, obtained by AFM, on the FIB milling time. One can see that it is close to linear for the times less than 20 s and then saturates. This can be associated with the phenomenon of material redeposition during the FIB etching. According to this data to make the arrays of the nanochannels in microfluidic devices the etching time was chosen to 10 s. This time provided the minimal width and sufficient depth of the nanochannels for further ion transport properties studies.

After the characterization of the obtained system of micro- and nanochannels the silicon substrate should be sealed with a glass or polymer film to form a microfluidic device. This is a very important technological step determining the quality of the following ion transport measurements and the lifetime of the device. One of the simplest encapsulation methods is based on the use of a polymer film (PDMS, SU-8 etc.) as a cover layer (Yazda et al. 2017; van Kan et al. 2012). At the first stage, we also tried to seal the chips using PDMS (Evstrapov et al. 2012). For this purpose, the surface of the chip and a PDMS film were pretreated in oxygen plasma and brought into contact with each other to form covalent bonding. However, such types of microfluidic chips have a number of fundamental disadvantages. Firstly, this encapsulation method is very pressure sensitive, which leads to necessity to work with very low flow rates of working solutions. And secondly, due to the porous nature of polymers, the lifetime of these chips is limited due to the presence of leakage currents (Yazda et al. 2017).

To overcome these limitations, in this work we used anodic bonding for sealing the microfluidic devices with a glass plate. It is a well-established approach for creating reliable electrostatic sealing between the surface of silicon (silicon oxide) and a cover glass plate (Kanda et al. 1990; Li and Wang 2004). We used a 450 μm thick borosilicate glass as a cover plate, which roughness was about 5 nm. The six

round holes with a diameter of 2 mm were made in the plate by the electrochemical discharge machining (Arab et al. 2019) to form the inlets and the outlets for the working solution, as well as for electrodes insertion into the working area (see Fig. 1). Before the anodic bonding, the glass surface was consistently cleaned in toluene, acetone and chromium anhydride and then dried in an oven. The surface of a silicon chip was treated in toluene and acetone to remove organic contamination. A homemade machine was used for bonding with the following parameters: the current—(140–190) μA, the applied voltage—(800–950) V, the system temperature—(390–410) °C, the welding time—30 min. Finally, massive PDMS fittings were used to connect flexible tubings with working solution and external electrodes to the inlets and outlets of the chip (see Fig. 2e). The fittings were covalently bonded to the glass surface after pretreatment with oxygen plasma.

The obtained chips were monolithic microfluidic devices with embedded micro- and nanochannels. The main benefit of the described fabrication approach is the possibility to apply high pressures (up to several atmospheres) without device damage. The critical pressure for each specific chip was individual. However, we can assert that all devices were able to operate at pressure up to 2 atmospheres. Moreover, the devices can be reused after subsequent washing. One of our devices has been in operation for more than a year.

2.2 Investigation of the transport phenomena

To study the possibility of using the created nanochannel systems in various applications (for example, as biomimetic devices) we investigated their transport properties by measuring ionic conductivity (Esfandiar et al. 2017). Comparison of the results with the theoretical model allowed us to evaluate the final nanochannel dimensions after the bonding step. Using a two-channel syringe pump, an aqueous solution of potassium chloride of a given concentration was pumped into both microchannels of the device. After the solution injection into the chip, it was left to be impregnated with the solution for 10 h. During this time the channels had enough time to be soaked at both low and high concentrations of the solution. Then, freshly chlorinated silver-chloride electrodes were mounted into the chip and it was placed into a metal Faraday cage.

The ionic conductivity of the nanochannels was determined by measuring the voltammetric (I–V) dependencies in the potentiostatic mode. Figure 4a shows typical I–V curves acquired at 0.01 M concentration of KCl solution. It should be mentioned that at low electrolyte concentrations (less than 0.01 M) a hysteresis on I–V curves can be obtained (see Fig. 4a). This phenomenon is associated with the capacitive component in the resistance of the nanochannels, caused by the accumulation of the counter ions at their entrances during the rapid sweep of the applied potential (BardandL and Faulkner yyy). To eliminate this effect, it is necessary to increase the time of the measurements (see Fig. 4a). For all the measurements at different concentrations of the solution, we set the time corresponding to the linear I–V curve. It should be noted that its linear character was preserved even at high bias voltages (–1 ... + 1V). To measure the whole range of concentrations it usually took us about a week. Between the measurements, the chip was kept filled with DI water in a sealed box at a humidity close to 99%. The studied microfluidic chips demonstrated good reproducibility of electrometric measurements. For example, we re-measured one of the chips after 3 months storage and the results changed only by 10% (see Fig. 4b).

2.3 Numerical simulations

To analyze obtained experimental results and calculate effective dimensions of the nanochannels we developed the theoretical model of ion transport through the nanochannels based on the Uniform potential model, which is derived from the Navier-Stokes, Nernst-Planck, and Poisson equations (Ryzhkov et al. 2018, 2019, 2020).

We consider a cylindrical nanochannel of radius R_p and length L_p, which separates two reservoirs L (left) and R

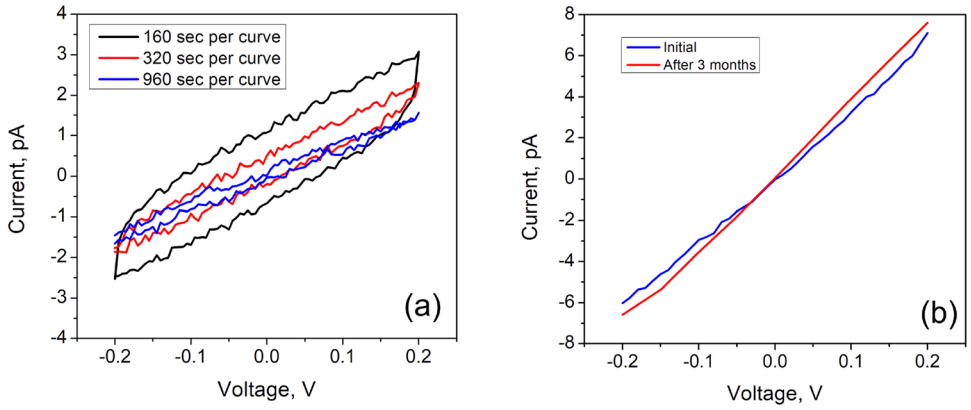

Fig. 4 **a** Current–voltage curves obtained in a microfluidic device at different recording times. **b** current–voltage curves obtained on the same chip under the same conditions with a difference of 3 months

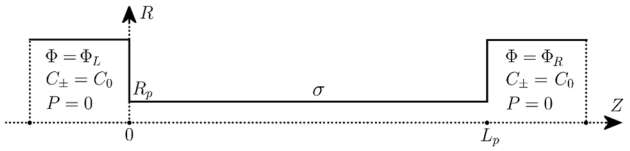

Fig. 5 The model of a cylindrical nanochannel separating two reservoirs

(right) with aqueous solution of the same monovalent and symmetric (1:1) electrolyte of concentration C_0 (Fig. 5). Consideration of the cylindrical geometry of the nanochannel was used because this geometry significantly simplifies the process of modeling and calculations, while the model does not lose its physical meaning. The motion of ions is induced by the electric field, which is imposed by specifying different potentials Φ_L and Φ_R in the reservoirs. It can be assumed without loss of generality that the potential in the left reservoir is zero. The reservoirs are maintained at equal constant pressures ($P_L = P_R$), which are taken zero for simplicity. The nanochannel surface is charged, and the surface charge density is denoted by σ. Further, it is assumed that the electric potential Φ, ion concentrations $C_\pm$, and pressure P are uniform in each cross-section of the pore, so they are functions of coordinate z directed along the pore. This assumption is valid when the pore radius is comparable or less than the Debye length (Mirkin and Amemiya 2015) determined by

$$\lambda = \sqrt{\frac{\varepsilon\varepsilon_0 R_g T}{2C_0 F^2}} \tag{1}$$

where ε_0 is the dielectric constant, ε is the relative dielectric permittivity, R_g is the universal gas constant, T is the temperature, and F is the Faraday constant.

The ionic conductivity G is the ratio of ionic current I to the applied potential difference U

$$G = \frac{I}{U}$$

Here $U = \Phi_L - \Phi_R$, so a positive voltage drop between left and right reservoirs induces positive current, i.e. positive charge is transported in the direction of electric field. The specific conductivity κ (S/m) of a cylindrical nanochannel is defined by

$$\kappa = G\frac{L_p}{\pi R_p^2} \tag{2}$$

Let us define the solvent volume flux (velocity) u_a, the ion fluxes $J_\pm$, the total ion flux $J = J_+ + J_-$, and the ionic charge flux $I' = J_+ - J_-$. The last is related to the ionic current by the formula $I = \pi R_p^2 F I'$. The dimensionless variables are introduced as follows

$$\begin{aligned} &Z = Lz,\ \Phi = \frac{R_g T}{F}\varphi,\ C_\pm = C_0 c_\pm,\ P = C_0 R_g T p,\\ &u_a = \frac{D_+}{L}u,\ J = \frac{D_+ C_0}{L}j,\ I' = \frac{D_+ C_0}{L}i \end{aligned} \tag{3}$$

Here, D_+ and D_- are the diffusion coefficients of cation and anion, respectively. Let us express the specific conductivity via the dimensionless charge flux and potential difference using (2) and (3):

$$\kappa = \frac{D_+ C_0 F^2}{R_g T}\frac{i}{\varphi_L - \varphi_R} \tag{4}$$

The dimensionless volume charge density equivalent to the surface charge density σ is defined by

$$X = \frac{2\sigma}{C_0 F R} \tag{5}$$

The latter is equal in magnitude and opposite in sign to the ionic volume charge density $c = c_+ - c_-$ due to the electroneutrality condition

$$X = c_- - c_+ \tag{6}$$

The equations of the Uniform potential model relate the volume flux, total ion flux, and ionic charge flux to the pressure, concentration, and potential gradients. For a nanochannel with the constant surface charge, they have the form Ref. Ryzhkov et al. (2019)

$$u = \frac{1}{8\alpha}\left[-\frac{dp}{dz} + X\frac{d\varphi}{dz}\right] \tag{7}$$

$$j = cu \quad + \frac{1}{2}\left[-(D+1)\frac{dc}{dz} + (X(D+1) + c(D-1))\frac{d\varphi}{dz}\right] \tag{8}$$

$$i = -Xu \quad + \frac{1}{2}\left[(D-1)\frac{dc}{dz} - (c(D+1) + X(D-1))\frac{d\varphi}{dz}\right] \tag{9}$$

Here, $c = c_+ + c_-$ is the total concentration of cations and anions; $D = D_-/D_+$ is the ratio of ion diffusion coefficients, and $\alpha = \mu D_+ (C_0 R_g T {R_p}^2)^{-1}$ is the dimensionless parameter determined by the viscosity of the solution. Equations (7)–(9) can be solved with respect to the derivatives dp/dz, dc/dz, $d\varphi/dz$ to obtain a system of three differential equations.

The conditions inside the nanochannel at the inlet from the left reservoir (at $z = 0$) and at the outlet to the right reservoir (at $z = 1$) are given by

$$p(0) = c(0) - 2c_0, \quad c(0) = \sqrt{X^2 + 4c_0^2}, \quad \varphi(0) = \varphi_0 \quad (10)$$

$$p(1) = c(1) - 2c_0, \quad c(1) = \sqrt{X^2 + 4c_0^2}, \quad \varphi(1) = \varphi_1 \quad (11)$$

Here, $\varphi_0 - \varphi_L$ and $\varphi_1 - \varphi_R$ are the Donnan potential jumps at the nanochannel inlet and outlet, respectively. The corresponding pressure and concentrations jumps are described by the first and second conditions in (10) and (11). Substituting the relations $c_{\pm}(0) = c_0 \exp(\mp(\varphi_0 - \varphi_L))$ and $c_{\pm}(1) = c_0 \exp(\mp(\varphi_1 - \varphi_R))$ into (6), we obtain the equations to determine the potentials φ_0 and φ_1

$$X = 2c_0 \sinh\left(\varphi_0 - \varphi_L\right), \; X = 2c_0 \sinh\left(\varphi_1 - \varphi_R\right) \quad (12)$$

The problem is solved numerically as follows. First, the initial approximations for fluxes u, j, i are set. Then the potentials ϕ_0 and φ_1 are determined from the equations (12) and boundary conditions (10) are set at $z = 0$. Then differential equations (7)–(9) are integrated numerically using Runge-Kutta-Merson method of 5th order from $z = 0$ to $z = 1$. The values of fluxes u, j, i are corrected in order to satisfy boundary conditions (12), and used for integration of equations at the next iteration. The iterations are performed until the values of fluxes converge to some constant values with required accuracy. Finally, the specific conductivity is calculated from (4).

It should be noted that if the pore radius is larger than the Debye length (1), the assumption of uniform potential and ion concentrations in the pore cross-section is no longer valid. However, the increase of pore radius decreases the effective volume charge (6), thus the pore size effects can still be described by the presented Uniform potential (UP) model.

The fitting of the measured experimental data to the theoretical model is performed by minimizing the sum of squared errors between theoretical and experimental data. For a one parameter fitting, the golden section method is used, while for multi-parameter fitting the Nelder–Mead method is employed (Nelder and Mead 1965).

3 Discussion

Figure 6 shows a typical experimental and theoretical dependencies of the ionic conductivity of the nanochannels on the concentration of KCl aqueous solution. The experimental points are measured using a chip with 15 parallel channels. At low concentrations of the working solution, the electrical double layers overlap inside the channels, thus, with concentration increasing the conductivity changes only slightly. However, at high concentrations the size of the double layers decreases, and the overlap disappears thus the conductivity increases accordingly. Simulations of based on the experimental data showed that the conductivity values correspond to the channels with effective diameters of 20 nm and the surface charge density of 1.5 mC/m^2. It should be noted that the calculated curve describes well the results at low concentrations; perhaps at high concentrations, it is necessary to take into account diffuse boundary layers. Moreover, we attribute the observed experimental effect of low conductivity at high concentration to the possible softening of the cover glass during anodic bonding and its subsequent flow into the nanochannels, which should reduce their effective dimensions. Additionally, during the bonding process electric charges could be introduced onto the surface of the channels, which can have strong influence on the ion currents.

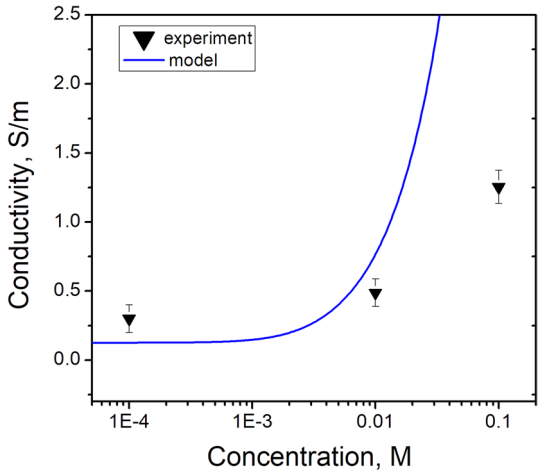

Fig. 6 The dependence of ionic conductivity of the nanochannels on the concentration of the working solution, as well as the result of the mathematical modeling. The measurement accuracy was 10–15%

4 Conclusions

We developed a technique for fabrication of silicon-glass microfluidic chips with a system of nanochannels connecting two independent volumes (2 half cells) using conventional optical lithography, plasma etching and FIB milling. To determine the regularities of FIB etching of nanochannels in silicon they were examined with SEM and AFM. It was experimentally revealed that the dependence of the FIB etching time on the width and the depth of the channels had complex behavior, which could be explained by the processes of material redeposition. However, the developed approach allows to reproducibly make the nanochannels with defined parameters. The obtained microchips were encapsulated with glass plates using the anodic bonding technique. Such approach provided the possibility to expand the lifetime of

the chips up to a year without significant changes of their characteristics. The ionic conductivity of the nanochannels was studied experimentally and using of the developed theoretical approach. Comparing the results we determined the effective diameter of the fabricated nanochannels and the surface charge density inside the channels to be 20 nm and 1.5 mC/m^2, respectively.

The proposed technique provides the tool to fabricate ensembles of nanochannels with a variable width and depth via varying the FIB milling time. Such microfluidic devices can find wide application in studies of the transport of both ions and various molecules through nanochannels. Further research in the field of application of the microfluidic chips developed in this study can be associated with the production of nanoporous DNA sequinators based on artificial pores, as well as with research in the field of controlled ion transport through the fabricated nanochannel. Additionally, metal contacts can be fabricated to the channel in order to implement an

ionic field-effect transistor, which is an advantage of the methodology proposed in the article.

5 Methods

In our work, we used a combination of optical and ion lithography methods to make microfluidic chips with nanochannels.

At the first stage of the technological process, thick inlet and outlet microchannels were made using conventional photolithography and plasma etching process. In brief, using direct laser writing lithography setup DWL 66 FS (Heidelberg instruments, Germany) the channels pattern was formed in an AZ MIR 701 photoresist layer applied by the spin coating to the surface of a silicon substrate with a low doping level. Exposed and developed photoresist was used as a mask for subsequent etching in CF4 plasma. The etching parameters were chosen as follows: flux 60 sccm, power 200 W. The time of the etching process was selected in such a way that the depth of the formed channels in a silicon was ~ 10 μm, which was monitored ex situ using an AmBios XP-1 solid-state profilometer. After the etching process, the photoresist layer was removed in a boiling ammonia-peroxide solution (1 NH_4OH:1 H_2O_2:3H_2O).

To form a network of nanochannels and control the FIB milling processes, a CrossBeam Neon40 (Carl Zeiss) crossed electron and an ion beam system was used. We used gallium ions at an accelerating voltage of 30 kV. An ion beam current of 10 pA was used for etching the network of nanochannels. The etching was carried out along a segment with a length of more than 10 μ and a width of 1 pixel. After the etching process the channels were visualized using an electron beam in the same system.

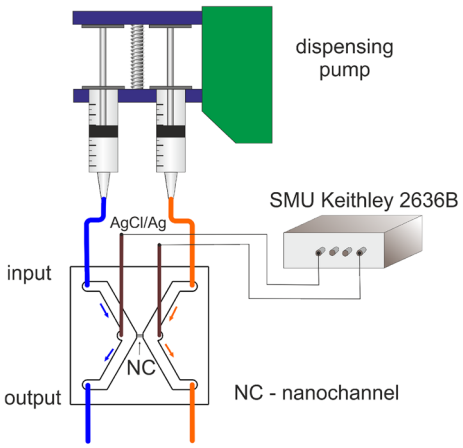

Fig. 7 Circuit diagram of a setup for studying the ion transport through nanochannels

To study the transport of ions through the nanochannels, we used the setup shown schematically in Fig. 7. A solution of potassium chloride in deionized MilliQ water was used as a working solution, the pH level in the solution in all experiments remained neutral (≈ 7). The solution was pumped into the microchannels of the chip using a two-channel syringe pump (Harvard Apparatus PHD 2000). Silver wires coated with a layer of silver chloride were used as measuring electrodes. The electrodes were mounted to the microfluidic system using custom PDMS adapters. The electrodes were connected to a source-meter (Keithley 2636B), with which all the electrical measurements were taken.

The chips were washed for reuse. The procedure for washing a microfluidic chip consists of several steps. In the first stage, the PDMS fittings are mechanically removed using a blade. Then the chip is immersed in a solution of chromic anhydride for a day to remove residues of PDMS and organic contaminants. Then the chip is washed repeatedly with isopropanol alcohol and deionized water. After this procedure the chip is dried at T = 110 °C. We do believe that this treatment ensures that chips are completely flushed and ready for use, which is also confirmed by reproducibility of measuring the ionic conductivity of the channels.

Acknowledgements The reported study was funded by RFBR according to the research Project No 19-08-00823 and the Ministry of Science and Higher Education of Russia (Project No. 075-15-2019-1896). The development of a technique for measuring the conductivity of ion channels was carried out the financial support of the Russian Science Foundation (Project No. 19-79-00095). The authors also express their gratitude to the resource center of SPBU "Optical and Laser Materials Research" and "Interdisciplinary Resource Centre for Nanotechnology". A.S. Bukatin and I.S. Mukhin thanks for financial support in the formation of microfluidic chips the Russian Science Foundation (Project No. 20-74-10117).

Author Contributions DL conceptualization, methodology, formal analysis, writing and original draft preparation, visualization, project administration, funding acquisition. GM investigation. IR software, formal analysis, theoretical model. AM resources, sample synthesis. KS resources, sample synthesis. VS AFM investigation. MP writing and original draft preparation. IT supervision. PA investigation. AE methodology, validation. AB validation, review and editing, funding acquisition. IM project administration, funding acquisition.

Declarations

Conflict of interest The authors declare that they have no known competing financial interests or personal relationships that could have appeared to influence the work reported in this paper.

References

Arab J, Adhale P, Mishra DK, Dixit P (2019) Micro array hole formation in glass using electrochemical discharge machining. Procedia Manuf 34:349–354. https://doi.org/10.1016/j.promfg.2019.06.174

Bardand LA, Faulkner R (1980) Electrochemical methods, fundamentals and applications. Wiley, NewYork

Chen Y (2015) Nanofabrication by electron beam lithography and its applications: a review. Microelectron Eng 135:57–72. https://doi.org/10.1016/j.mee.2015.02.042

Chen X, Zhang L (2018) Review in manufacturing methods of nanochannels of bio-nanofluidic chips. Sens Actuat B: Chem 254:648–659. https://doi.org/10.1016/j.snb.2017.07.139

de la Escosura-Muñiz A, Merkoçi A (2012) Nanochannels preparation and application in biosensing. ACS Nano 6(9):7556–7583. https://doi.org/10.1021/nn301368z

Esfandiar A, Radha B, Wang FC, Yang Q, Hu S, Garaj S, Nair RR, Geim AK, Gopinadhan K (2017) Size effect in ion transport through Angstrom-scale slits. Science 358(6362):511–513. https://doi.org/10.1126/science.aan5275

Evstrapov A, Mukhin I, Bukatin A, Kukhtevich I (2012) Ion and electron beam assisted fabrication of nanostructures integrated in microfluidic chips. Nucl Inst Methods Phys Res Sect B Beam Interact Mater Atoms 282:145–148. https://doi.org/10.1016/j.nimb.2011.08.035

Favre I, Moczydlowski E, Schild L (1996) On the structural basis for ionic selectivity among Na+, K+, and Ca2+ in the voltage-gated sodium channel. Biophys J 71(6):3110–3125. https://doi.org/10.1016/S0006-3495(96)79505-X

Guan W, Reed MA (2012) Electric field modulation of the membrane potential in solid-state ion channels. Nano Lett 12(12):6441–6447. https://doi.org/10.1021/nl303820a

Guo LJ (2007) Nanoimprint lithography: methods and material requirements. Adv Mater 19(4):495–513. https://doi.org/10.1002/adma.200600882

Han W, Chen X (2019) Nano-electrokinetic ion enrichment of highly viscous fluids in micro-nanochannel. Chem Eng Process Process Intensif 143:107626

Han W, Chen X (2020) Nano-electrokinetic ion enrichment in a micro-nanofluidic preconcentrator with nanochannel's cantor fractal wall structure. Appl Nanosci 10(1):95–105

Han W, Chen X (2020) A novel design of nanochannel structure in a micro-nanofluidic preconcentrator for electrokinetic ion enrichment. J Braz Soc Mech Sci Eng 42(1):1–9

Han W, Chen X (2020) A review: applications of ion transport in micro-nanofluidic systems based on ion concentration polarization. J Chem Technol Biotechnol 95(6):1622–1631

Hao Z, Zhang Q, Xu X, Zhao Q, Wu C, Liu J, Wang H (2020) Nanochannels regulating ionic transport for boosting electrochemical energy storage and conversion: a review. Nanoscale 12(30):15923–15943. https://doi.org/10.1039/D0NR02464C

Hou G, Peng Z, Tian Y, Zhang H, Jiang L (2013) Applications of polymer single nanochannels in biosensors. Chin Sci Bull 58(13):1473–1482. https://doi.org/10.1007/s11434-013-5788-0

Kanda Y, Matsuda K, Murayama C, Sugaya J (1990) The mechanism of field-assisted silicon-glass bonding. Sens Actuat A: Phys 23(1–3):939–943. https://doi.org/10.1016/0924-4247(90)87064-P

Kowalczyk SW, Blosser TR, Dekker C (2011) Biomimetic nanopores: learning from and about nature. Trends Biotechnol 29(12):607–614. https://doi.org/10.1016/j.tibtech.2011.07.006

Kurita R, Niwa O (2016) Microfluidic platforms for DNA methylation analysis. Lab Chip 16(19):3631–3644. https://doi.org/10.1039/C6LC00829A

Le T, Shimizu H, Morikawa K (2020) Advances in label-free detections for nanofluidic analytical devices. Micromachines 11(10):885. https://doi.org/10.3390/mi11100885

Li G, Wang L (2004) Influence of bonding parameters on electrostatic force in anodic wafer bonding. Thin Solid Films 462–463:334–338. https://doi.org/10.1016/j.tsf.2004.05.084

Ma T, Balanzat E, Janot J-M, Balme S (2019) Single conical track-etched nanopore for a free-label detection of OSCS contaminants in heparin. Biosens Bioelectron 137:207–212. https://doi.org/10.1016/j.bios.2019.05.005

Ma T, Balanzat E, Janot J-M, Balme S (2019) Nanopore functionalized by highly charged hydrogels for osmotic energy harvesting. ACS Appl Mater Interfaces 11(13):12578–12585. https://doi.org/10.1021/acsami.9b01768

Ma T, Janot J, Balme S (2020) Track-etched nanopore/membrane: from fundamental to applications. Small Methods 4(9):2000366. https://doi.org/10.1002/smtd.202000366

McDonald JC, Whitesides GM (2002) Poly(dimethylsiloxane) as a material for fabricating microfluidic devices. Acc Chem Res 35(7):491–499. https://doi.org/10.1021/ar010110q

Medina-Sánchez M, Miserere S, Cadevall M, Merkoçi A (2016) Enhanced detection of quantum dots labeled protein by simultaneous bismuth electrodeposition into microfluidic channel. Electrophoresis 37(3):432–437. https://doi.org/10.1002/elps.201500288

Menard LD, Ramsey JM (2011) Fabrication of sub-5 nm nanochannels in insulating substrates using focused ion beam milling. Nano Lett 11(2):512–517. https://doi.org/10.1021/nl103369g

Mills KL, Huh D, Takayama S, Thouless MD (2010) Instantaneous fabrication of arrays of normally closed, adjustable, and reversible nanochannels by tunnel cracking. Lab Chip 10(12):1627. https://doi.org/10.1039/c000863j

Mirkin MV, Amemiya S (2015) Nanoelectrochemistry. CRC Press, Boca Raton

Mokkapati VRSS, Di Virgilio V, Shen C, Mollinger J, Bastemeijer J, Bossche A (2011) DNA tracking within a nanochannel: device fabrication and experiments. Lab Chip 11(16):2711. https://doi.org/10.1039/c1lc20075e

Mukhin I, Fadeev I, Zhukov M, Dubrovskii V, Golubok A (2015) Framed carbon nanostructures: synthesis and applications in functional SPM tips. Ultramicroscopy 148:151–157. https://doi.org/10.1016/j.ultramic.2014.10.008

Nam S-W, Lee M-H, Lee S-H, Lee D-J, Rossnagel SM, Kim K-B (2010) Sub-10-nm nanochannels by self-sealing and self-limiting atomic layer deposition. Nano Lett 10(9):3324–3329. https://doi.org/10.1021/nl100999e

Nelder JA, Mead R (1965) A simplex method for function minimization. Comp J 7(4):308–313

Noakes MT, Brinkerhoff H, Laszlo AH, Derrington IM, Langford KW, Mount JW, Bowman JL, Baker KS, Doering KM, Tickman BI, Gundlach JH (2019) Increasing the accuracy of nanopore

DNA sequencing using a time-varying cross membrane voltage. Nat Biotechnol 37(6):651–656. https://doi.org/10.1038/s41587-019-0096-0

O'Brien MJ, Bisong P, Ista LK, Rabinovich EM, Garcia AL, Sibbett SS, Lopez GP, Brueck SRJ (2003) Fabrication of an integrated nanofluidic chip using interferometric lithography. J Vac Sci Technol B: Microelectron Nanometer Struct 21(6):2941. https://doi.org/10.1116/1.1625964

Ou X, Chen P, Huang X, Li S, Liu B (2020) Microfluidic chip electrophoresis for biochemical analysis. J Sep Sci 43(1):258–270. https://doi.org/10.1002/jssc.201900758

Ouyang W, Han J (2019) Universal amplification-free molecular diagnostics by billion-fold hierarchical nanofluidic concentration. Proc Natl Acad Sci 116(33):16240–16249. https://doi.org/10.1073/pnas.1904513116

Payandeh J, Gamal El-Din TM, Scheuer T, Zheng N, Catterall WA (2012) Crystal structure of a voltage-gated sodium channel in two potentially inactivated states. Nature 486 (7401) 135–139. https://doi.org/10.1038/nature11077. http://www.nature.com/articles/nature11077

Peng R, Li D (2016) Fabrication of polydimethylsiloxane (PDMS) nanofluidic chips with controllable channel size and spacing. Lab Chip 16(19):3767–3776. https://doi.org/10.1039/C6LC00867D

Picallo CB, Gravelle S, Joly L, Charlaix E, Bocquet L (2013) Nanofluidic osmotic diodes: theory and molecular dynamics simulations. Phys Rev Lett 111(24):2444501. https://doi.org/10.1103/PhysRevLett.111.244501

Ramsden JJ (2016) Nanotechnology, Elsevier. https://www.elsevier.com/books/nanotechnology/ramsden/978-0-323-39311-9. https://linkinghub.elsevier.com/retrieve/pii/C20140039123

Ryzhkov II, Vyatkin AS, Medvedeva MI (2019) Modelling of electrochemically switchable ion transport in nanoporous membranes with conductive surface. J Siberian Federal Univ Math Phys 579–589 https://doi.org/10.17516/1997-1397-2019-12-5-579-589. http://www.journal.sfu-kras.ru/en/article/125576

Ryzhkov II, Lebedev DV, Solodovnichenko VS, Minakov AV, Simunin MM (2018) On the origin of membrane potential in membranes with polarizable nanopores. J Membr Sci 549:616–630. https://doi.org/10.1016/j.memsci.2017.11.073

Ryzhkov II, Vyatkin AS, Mikhlina EV (2020) Modelling of conductive nanoporous membranes with switchable ionic selectivity. Membr Membr Technol 2(1):10–19. https://doi.org/10.1134/S2517751620010072

Shi X, Verschueren DV, Dekker C (2018) Active delivery of single DNA molecules into a plasmonic nanopore for label-free optical sensing. Nano Lett 18(12):8003–8010. https://doi.org/10.1021/acs.nanolett.8b04146

Siria A, Poncharal P, Biance A-L, Fulcrand R, Blase X, Purcell ST, Bocquet L (2013) Giant osmotic energy conversion measured in a single transmembrane boron nitride nanotube. Nature 494(7438):455–458. https://doi.org/10.1038/nature11876

Sparreboom W, van den Berg A, Eijkel JCT (2009) Principles and applications of nanofluidic transport. Nat Nanotechnol 4(11):713–720. https://doi.org/10.1038/nnano.2009.332

Tagliazucchi M, Szleifer I (2015) Transport mechanisms in nanopores and nanochannels: can we mimic nature? Mater Today 18(3):131–142. https://doi.org/10.1016/j.mattod.2014.10.020

van Kan JA, Zhang C, Perumal Malar P, van der Maarel JRC (2012) High throughput fabrication of disposable nanofluidic lab-on-chip devices for single molecule studies. Biomicrofluidics 6(3):036502. https://doi.org/10.1063/1.4740231. http://aip.scitation.org/doi/10.1063/1.4740231

Wang P, Wang M, Liu F, Ding S, Wang X, Du G, Liu J, Apel P, Kluth P, Trautmann C, Wang Y (2018) Ultrafast ion sieving using nanoporous polymeric membranes. Nat Commun 9(1):569. https://doi.org/10.1038/s41467-018-02941-6

Wang Y, Yang Q, Wang Z (2015) The evolution of nanopore sequencing, Front Genet 5. https://doi.org/10.3389/fgene.2014.00449. http://journal.frontiersin.org/article/10.3389/fgene.2014.00449/abstract

Wu W, Walmsley RG, Li W-D, Li X, Williams RS (2012) Nanoimprint lithography with 60 nm overlay precision. Appl Phys A 106(4):767–772. https://doi.org/10.1007/s00339-012-6775-z

Xia D, Yan J, Hou S (2012) Fabrication of nanofluidic biochips with nanochannels for applications in DNA analysis. Small 8(18):2787–2801. https://doi.org/10.1002/smll.201200240

Xu Y, Matsumoto N (2015) Flexible and in situ fabrication of nanochannels with high aspect ratios and nanopillar arrays in fused silica substrates utilizing focused ion beam. RSC Adv 5(62):50638–50643. https://doi.org/10.1039/C5RA06306J

Xu Z, Zhu Z, Li N, Tian Y, Jiang L (2018) Continuous in situ extraction toward multiphase complex systems based on superwettable membrane with micro-/nanostructures. ACS Nano 12(10):10000–10007. https://doi.org/10.1021/acsnano.8b04328

Yazda K, Tahir S, Michel T, Loubet B, Manghi M, Bentin J, Picaud F, Palmeri J, Henn F, Jourdain V (2017) Voltage-activated transport of ions through single-walled carbon nanotubes. Nanoscale 9(33):11976–11986. https://doi.org/10.1039/C7NR02976D

Zhang H, Xu Y, Fohlerova Z, Chang H, Iliescu C, Neuzil P (2019) LAMP-on-a-chip: revising microfluidic platforms for loop-mediated DNA amplification. TrAC Trends Anal Chem 113:44–53. https://doi.org/10.1016/j.trac.2019.01.015

Zhou J (2011) Controllable fabrication of enclosed micro/nanochannels via polymethyl methacrylate pattern as sacrificial template and capillary effect. J Micro/Nanolithogr MEMS, MOEMS 10(4):049701. https://doi.org/10.1117/1.3665215. http://nanolithography.spiedigitallibrary.org/article.aspx?doi=10.1117/1.3665215

Zhu Z, Wang D, Tian Y, Jiang L (2019) Ion/molecule transportation in nanopores and nanochannels: from critical principles to diverse functions. J Am Chem Soc 141(22):8658–8669. https://doi.org/10.1021/jacs.9b00086